Unraveling the Internal Structure of 3D Printed Stimuli-Responsive Materials Using a Molecular Probe

Xiaowo Kang[1†], Weijun Wu[1†*], Yu Hu[1], Xindi Liu[1], Wenhui Wang[1], Qiao Song[2], Yu Xiong[3], Yinyin Bao[4], Lu Zhang[1], Bin Zhao[5], Hongyan Jiang[5], Mingxi Yao[1], and Zhi Luo[1*]

Affiliations

[1] Guangdong Provincial Key Laboratory of Advanced Biomaterials, Department of Biomedical Engineering, Southern University of Science and Technology, Shenzhen 518055, Guangdong, P.R. China.

[2] Shenzhen Grubbs Institute, Southern University of Science and Technology, Shenzhen 518055, China.

[3] College of Materials Science and Engineering, Shenzhen University, Shenzhen, 518061 China.

[4] Department of Chemistry and Applied Biosciences, ETH Zurich; Zurich 8093, Switzerland.

[5] Department of Chemistry, Southern University of Science and Technology, Shenzhen 518055, Guangdong, P.R. China.

[†] These authors contributed equally to this work.

[*] Corresponding authors: wuwj@sustech.edu.cn, luoz@sustech.edu.cn

Abstract

Stimuli-responsive 3D printing, or 4D printing, offers unparalleled potential in various research fields, enabling the combination of complicated mechanical design with programmable functionalities. The switchable polymer network structures, e.g., crystalline domains, free volume, and phase separation, are the key to achieving macroscopic responsiveness. However, despite a growing repertoire of new materials, most studies rely on rudimentary imaging techniques to visualize the materials' shape change under external stimuli. Seldomly could such macroscopic behavior be correlated with the nanoscopic structures and dynamics of polymers. Here, leveraging the AIE phenomena, we introduce a novel method that can offer direct insights into the network structures and the chain mobility of the printed polymers. We developed a new photo-polymerizable polyurethane with multiple responsive characteristics, including temperature, mechanical strain, and pH, as an example of 4D printing materials. By embedding AIEgen in the polymer matrix, we demonstrated that the emission intensity and wavelength can serve as reporters and correlate the intramolecular motions of the AIEgen with the stimuli-responsive properties of the polymers. These observations were confirmed by small-angle X-ray scattering revealing the underpinning structural evolution. With potential applications for real-time structural monitoring, this study provides a new tool for the characterization of 4D printed materials.

Introduction

3D printing techniques such as digital light processing (DLP), holds immense promise across diverse fields due to its ability to fabricate sophisticated and customizable structures[1,2]. A recent concept of 'fourth dimension' has emerged[3,4], where the printed objects' shape, properties, or functionality can dynamically change over time in response to external stimuli such as pH, temperature, light, and strains[5–8]. Unlike traditional manufacturing, the 4D printing technique transcends mere fabrication, enabling precise and sequential movement control of complex structures in various applications from medical devices[9–11], sensors[12], soft robotics[13,14], to metamaterials[15,16].

At the molecular and nanoscale level, the incorporation of dynamically switchable structure units into the polymer networks are the key to the development of stimuli-responsive 3D printing materials[17,18]. Diverse principles have been employed, such as the induction of phase separation[19], tuning of phase transition temperatures[20], and the integration of light and pH-sensitive functional groups[21]. For example, the phase separation mechanism has been harnessed in numerous research to generate hierarchical structures, imparting switchable mechanical properties to 3D printed materials[22]. Levkin and coworkers demonstrated that the phase separation can not only endow the 3D printed polymers with high strength and toughness, but also offer shape memory properties due to the formation of hard domains with a high glass transition temperature (T_g)[23]. Deore et. al. reported a polymerization-induced phase separation strategy to control the spatial distribution of different material phases and achieved a range of 3D objects with diverse functionalities[24]. Furthermore, the structure of nanoscale crystalline and amorphous domains plays an important role in the stimuli-responsive properties of these materials[25]. For instance, polyurethane (PU) elastomers exhibit soft domains in a rubbery state at room temperature due to their lower T_g, while hard domains appear semi-crystalline or glassy with a higher T_g. Consequently, PU based materials with temperature-responsive mechanical properties have been designed and printed, allowing the fabrication of various bionic actuators[26], thermoelectric generators[27] and flexible sensors[28].

The engineering of polymer network structure is also important for the 4D printing of pH- and temperature-responsive materials. One notable example is the fabrication of self-expandable medical

devices for intravascular and gastrointestinal applications[29,30]. Utilizing polymer structures with shape memory properties, these devices can be precisely designed to enable controlled shape change in response to the body temperature[31–33]. It has been proposed that the shape memory behavior are directly related to the viscosity and relaxation property of the polymer networks[34], and can be considered as a mixture of different frozen and active phases, where the T_g determines the changes in the volume fraction of each phase. When the rubber phase transits into the frozen phase, the deformation characteristics in the rubber phase is stored after releasing the external load. Similarly, another important example is the development of smart drug delivery devices[35,36], where the controllable relaxation of polymer networks is the key to optimizing the drug release kinetics. With the swelling or dissolution of the polymers, therapeutic agents can be released in response to specific pH levels within the body[29,37], resulting in improved drug efficacy and minimized side effects.

Despite the significance of the nanoscale polymer structure engineering, currently, most studies focus solely on reporting the macroscopic behavior of 4D printed materials. These investigations often rely on simple optical imaging methods, which lack the capability to provide molecular information about the material's internal structure and the dynamics of the polymer networks. Only few studies have utilized small-angle X-ray scattering (SAXS) to determine the transition of crystalline domains in the printed materials[38–40]. However, the penetration depth of the X-ray limits its application to very thin specimens (typically less than 1 mm) and it is difficult to perform a full-size imaging of complex samples with SAXS. In addition to experimental techniques, the stimuli-responsiveness structural change could, in principle, also be reconstructed through finite element simulations[41]. However, 3D printed materials often do not obey linear elasticity and the complex geometry and loading profiles could lead to computationally consuming calculations with inaccurate results. These limitations have sparked the need for novel characterization methods to directly measure material’s structure changes, rather than relying on strain field calculations. To the best of our knowledge, currently, there is no technique that allows the *in situ* imaging of the internal structures within 4D printed polymer networks.

Aggregation-induced emission luminogen (AIEgen) is a type of unique luminescent material with great potential in biosensing[42], imaging[43,44], and photonics[45]. Unlike conventional fluorophores,

these molecules exhibit enhanced photoluminescence when aggregated, a phenomenon known as the AIE effect[46–48]. The distinctive behavior is closely linked to the molecular dynamics of AIEgen, where the restricted intramolecular motions in condensed states, such as rotations and vibrations, activates the radiative decay[49]. By doping AIE molecules into polymer matrices and investigating the emission profile under different conditions, it is possible to reveal how microscopic structures and dynamics of the polymers influence the intramolecular motions of AIEgens[50]. Therefore, the AIE fluorescence could be employed as an efficient yet simple tool to understand essential structure information of the polymers[51,52], including the nanoscale phase separation, polymer chain dynamics, flexibility, molecular weights and polarity. For example, using AIEgen as a probe, Qiu et. al. demonstrated the accurate determination of T_g for various polymer films, which can be well correlated with differential scanning calorimetry (DSC) analysis[53].

In this study, we present a novel AIEgen probe based monitoring method to visualize the internal structure changes in 4D printed materials. We first synthesized a photo-polymerizable PU that is responsive to various types of external stimuli, such as pH, temperature, and strain, as a general example for stimuli-responsive 3D printing materials (Figure 1). By incorporating near-infrared fluorescent AIEgen, TPAPY-SH, within the printed material, we demonstrate that switchable emission profiles could be observed along with the change of the ordering, dynamics, and steric effects of polymer networks. As a result, the AIEgens serve as a versatile reporter of microscopic free volume and polymer chain mobility, allowing for simple yet precise detection of the polymer structure evolution in response to external stimuli. This AIE-assisted monitoring technique holds great promise as a universal method to evaluate the stimuli-responsive mechanisms of 3D printed smart materials offering valuable insights into the microscopic dynamics *in situ*.

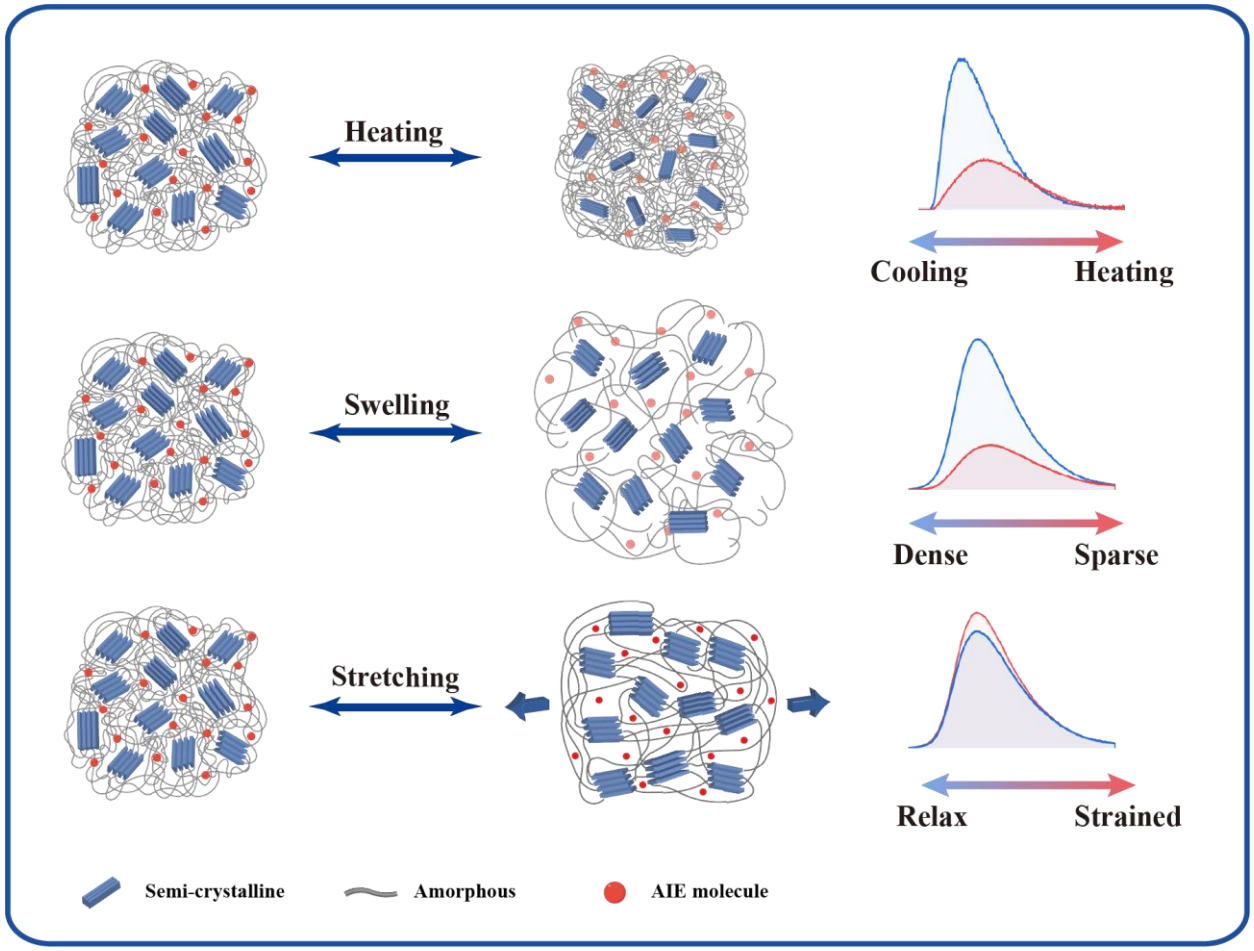

Figure 1. Scheme of in situ monitoring of structure change within 4D printed material under external stimuli using an AIEgen probe.

Results and Discussion

DLP printable multi-responsive polyurethane

A facile one-pot two step reaction was performed for the preparation of the functionalized PU. The synthesis was conducted overnight under ambient condition, i.e., room temperature in dimethylformamide, yielding more than 20 g yield per batch. This indicated the scale-up potential of the polymer resin. As shown in Figure 2A, a novel urethane main chain structure was achieved by the polycondensation of *N*-methyldiethanolamine (MDEA) and hexamethylene diisocyanate (HDI). These two monomers impart different properties to the printed material. First, MDEA contributes to the pH responsiveness owing to the presence of tertiary amines that can be protonated under acid conditions. With a pKa of 8.5, MDEA has also been widely utilized for CO_2 capturing applications[54,55]. Therefore,

the as prepared PU material could be potentially responsive to both pH and CO_2. While MDEA is relatively hydrophilic, the second monomer HDI is hydrophobic and highly reactive allowing for the formation of urethane bonds robustly. The efficient synthesis resulted in polymer chains with high molecular weight, and thus good elasticity of the printed polymer networks. At the same time, the coexistence of crystalline and amorphous domains in synthesized PU would contribute to the temperature responsiveness. The hydrogen bonding interaction between the two monomers could lead to hard segments featuring ordered crystalline regions, which will potentially alter (ultimately causing a change in the materials') the mechanical properties, such as the Young's modulus, rigidity, as well as T_g and thermal expansion coefficient of the printed materials. Additionally, the PU polymer is end functionalized with hydroxyethyl methacrylate, whose conversion degree will dictate cross-linking density and the network structures.

The polymer was characterized by ^{1}H NMR spectroscopy (Figure S1), which showed an averaged molecular weight of 12000 g·mol^{-1}. As shown in Figure 3A, by DSC analysis, the polymer showed a T_g of -10.7 ℃ and a T_m of 55.1 ℃. Above 55.1 ℃, the PU is a viscous liquid, while below this temperature, it turns solid due to intermolecular interactions and dense chain packing. While long polymer chain can potentially provide good elasticity to the printed material (Figure 2B), it also results in high viscosity which hinders high-resolution printing in common DLP setups. To decrease the viscosity and T_m, a commonly used reactive solvent, *N*-vinylpyrrolidone (NVP)[56] was added to dilute the resin. Nevertheless, the high amount of NVP would compromise mechanical properties, leading to a reduction in Young's modulus and an increase in brittleness in the printed materials.

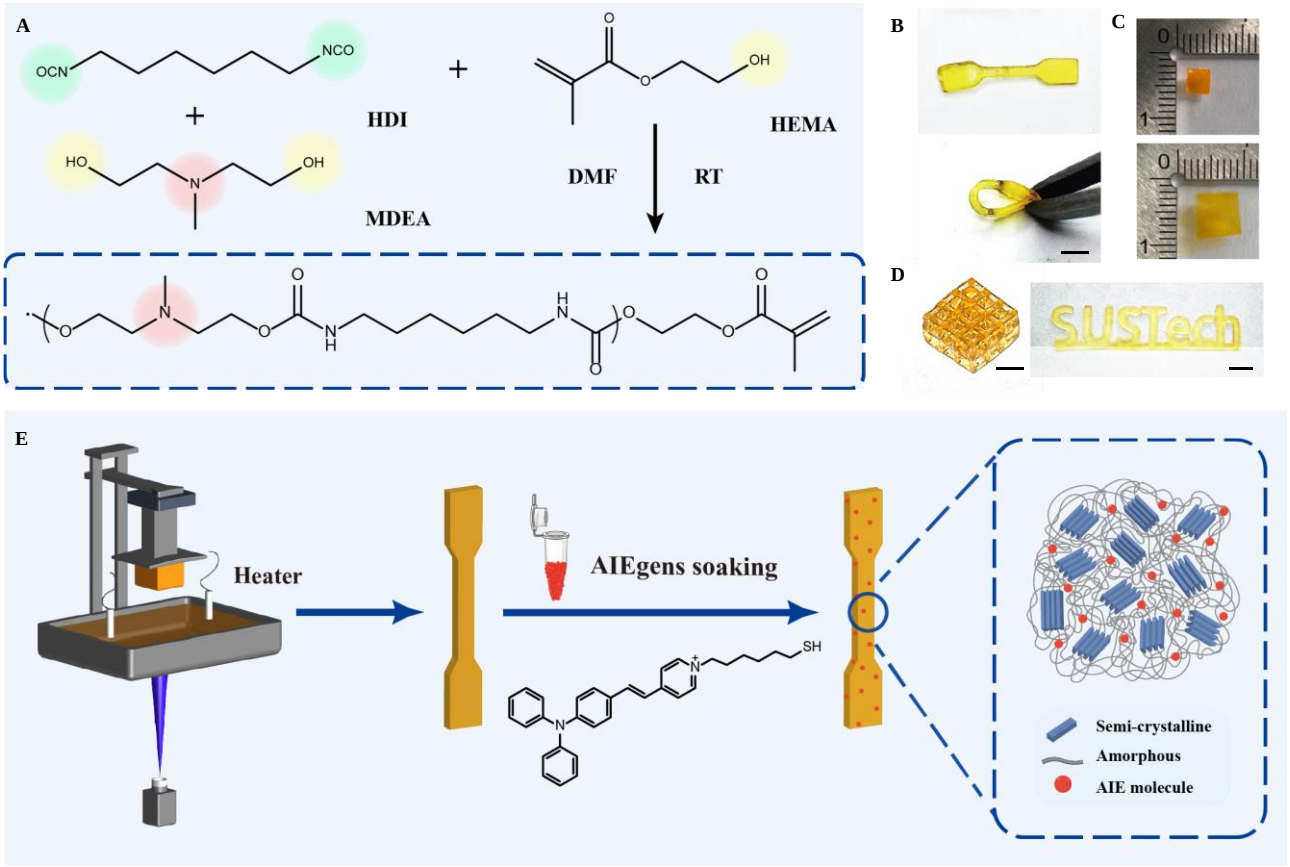

Figure 2. Chemical synthesis and 3D printing process of stimuli-responsive elastomers. A) The design and chemical structure of a photo-polymerizable and multiple stimuli-responsive polyurethane (PU). B) Highly flexible 3D printed dumbbell-shaped elastomer. C) The 3D printed PU before and after swelling in hydrochloric acid solution with potassium chloride of pH=1. D) 3D printed lattice structure and letters "SUSTech" using the PU. Scale bar = 5 mm. E) Illustration of the fabrication of the PU by a customized DLP printer with a temperature control platform and post-incorporation.

Therefore, to minimize the fraction of NVP and to further reduce the resin, we modified a DLP printer with a customized heating platform[57–60] (Figure S2), to realize a precise heating control and allow stable printing at elevated temperature (up to 110 °C). This effectively lowered the resin viscosity to a suitable range for DLP printing and at the same time facilitated the crosslinking efficiency and thus reduces the printing time. For optimized printing quality, we prepared the PU resin using 30% NVP and set the printing temperature to 90 °C with 20 mW/cm² light intensity, 30 s layer exposure time, and 0.05 mm slice thickness using a commercial DLP printer. As shown in Figure 2B-D, various complex shapes, e.g., lattice structure and letter objects, could be readily printed. The printed material demonstrated favorable elastomeric mechanical properties, with a yield strength of 2.7 ± 0.02 MPa and a notable strain capacity of 191%. Furthermore, as expected, the PU material also exhibited

significant swelling capability (up to 3 times in each dimension) when exposed to hydrochloric acid solution (pH = 3, Figure 2C). Overall, a 3D printable PU material with multiple stimuli-responsiveness has been successful obtained.

AIEgen-incorporated 3D printed elastomer

A thiolated AIEgen derived from triphenylamine, TPAPY-SH[61], was synthesized as the probe molecule to be integrated in the 3D printed materials. The detailed synthetic steps and characterization are described in the Supplementary Information. We first examined the absorption and fluorescence spectra of TPAPY-SH. As shown in Figure S3 and S4, the absorption and fluorescence maximum of TPAPY-SH in CH_2Cl_2 are 475 and 678 nm, respectively. We further used a mixed solvent (DMSO/water) with different water fractions as a solvent system to evaluate the AIE features of TPAPY-SH. As depicted in Figure S5, the fluorescence of TPAPY-SH in pure DMSO solution was very strong. As the fraction of water increased to 50%, the molecular fluorescence began to decrease. And then with the fraction of water increasing to 99%, the fluorescence of TPAPY-SH gradually increased, and finally became higher than the fluorescence in pure DMSO solution, confirming typical AIE characteristics. The emission enhancements could be explained by the restriction of rotational motions following aggregate formation.

Both the excitation and emission wavelengths of TPAPY-SH are above 405 nm, avoiding the potential interference with DLP printing process, which typically relies on UV or deep blue light with a wavelength around 365 or 405 nm. Therefore, it is possible to integrate TPAPY-SH in the printed materials either by direct resin formulation prior to printing or by post-printing soaking (Figure 2E). Furthermore, the incorporation of a hexane-thiol functional group not only leads to better compatibility of TPAPY-SH with various types of polymer resins, but also allows the covalent attachment onto the polymer networks through Michael addition reaction.

To evaluate the emission properties of TPAPY-SH within the polymer matrix, we prepared 3D printed film samples with a thickness of 1 mm, followed by soaking into a solution containing the AIE molecules. The photoluminescence quantum yield (PLQY) of TPAPY-SH within the elastomer is

approximately 46%, a marked enhancement when compared with the inherent PLQY of the AIEgen small molecule, which remains too faint to be quantified under the same condition. As shown in Fig S5, one immediately notices that the luminance of AIE molecules in printed materials showed much higher intensity compared to that of the solid states. Furthermore, a significant blue shift (from 670 nm to 605 nm) of the emission peak was observed. To test whether such shift is due to the polarity change in the environment provided by the polymers, we then measured the emission wavelength of the same AIEgen molecule TPAPY-SH in various organic solvents, including ethanol, dimethyl sulfoxide, dichloromethane, ethyl acetate, toluene, and hexane. Interestingly, despite the notably higher molecule concentration (2 mg/mL) within the solvent in comparison to the material film (0.25 mg/mL), the fluorescence intensities of all the solution remain inferior to that of the film. In general, the emission peaks of TPAPY-SH solution were more blue-shifted in solvents with lower polarity. However, despite the wide range of solvents, none of the emission maximum from solution was lower than 625 nm. These results potentially suggest that both the shift[62] and the enhancement of the fluorescent intensity cannot be solely explained by the polarity changes; instead, they are most likely arisen from conformational restrictions of the AIE molecules within the polymer network.

Correlation between polymer chain mobility and the AIEgen emission

To visualize the sensitivity of the AIEgen emission to temperature within 3D printed polymer, we printed a dog bone-shaped specimen and recorded its fluorescent emission images *in situ* during heating (Figure 3B-C). A remarkable transition in color from orange to brown could be observed as the temperature increased, signifying a decrease in the fluorescence intensity.

To quantitatively correlate the emission profile with the temperature and structure of the polymers, we performed *in situ* fluorescent intensity and lifetime measurements at different temperatures. The fluorescence intensity was recorded using a FLS 1000 photoluminescence spectrometer across a temperature range from 193 K to 373 K, encompassing both T_g and T_m of the material. As shown in Figure 3D-G, with increasing temperature, both the fluorescence intensity and lifetime exhibited a declining trend with the intensity being 5.49×10^5 at 193 K and 1.83×10^5 at 373 K, indicating that it is plausible to visualize the temperature responsive structural changes of the printed polymer with the

help of the AIE probes. The first possible explanation for such a decreased intensity at higher temperature could be due to the inherent temperature sensitivity of TPAPY-SH. As the temperature increased, a reduction in fluorescence is expected, which can be attributed to the enhanced rotation and vibration resulting from the absorption of thermal energy. We therefore performed the same *in situ* analysis on the TPAPY-SH molecule in solid state. As shown in Figure S6B, the fluorescent intensity did not change significantly with temperature. Therefore, the enhanced thermal motion of TPAPY-SH itself is not the main reason for the decreased emission of the printed material at elevated temperatures.

The second hypothesis is that the reduced emission is a direct reflection of the free volume change of the polymer networks resulting from the increased mobility of the polymer chain. Indeed, as shown in Figure 3E and G, the dependence of both the fluorescent intensity and lifetime was not linearly correlated to the temperature change. Three distinct temperature regions could be observed in the fluorescence intensity trends, with the transition region close to the T_g (-10.7 °C) and the T_m (55.1 °C) of the PU material. Below T_g, the polymer stays in the glassy states and the frozen domains restrict the intramolecular motion of the AIE molecule due to confined space. Therefore, there were no significant decrease of the fluorescence and lifetime. According to the cooperative motion and free volume theory, the decline of temperature could cause dramatic reduction in molecular mobility and the increase of density, which cannot provide sufficient free volume for molecules to move[63–65].

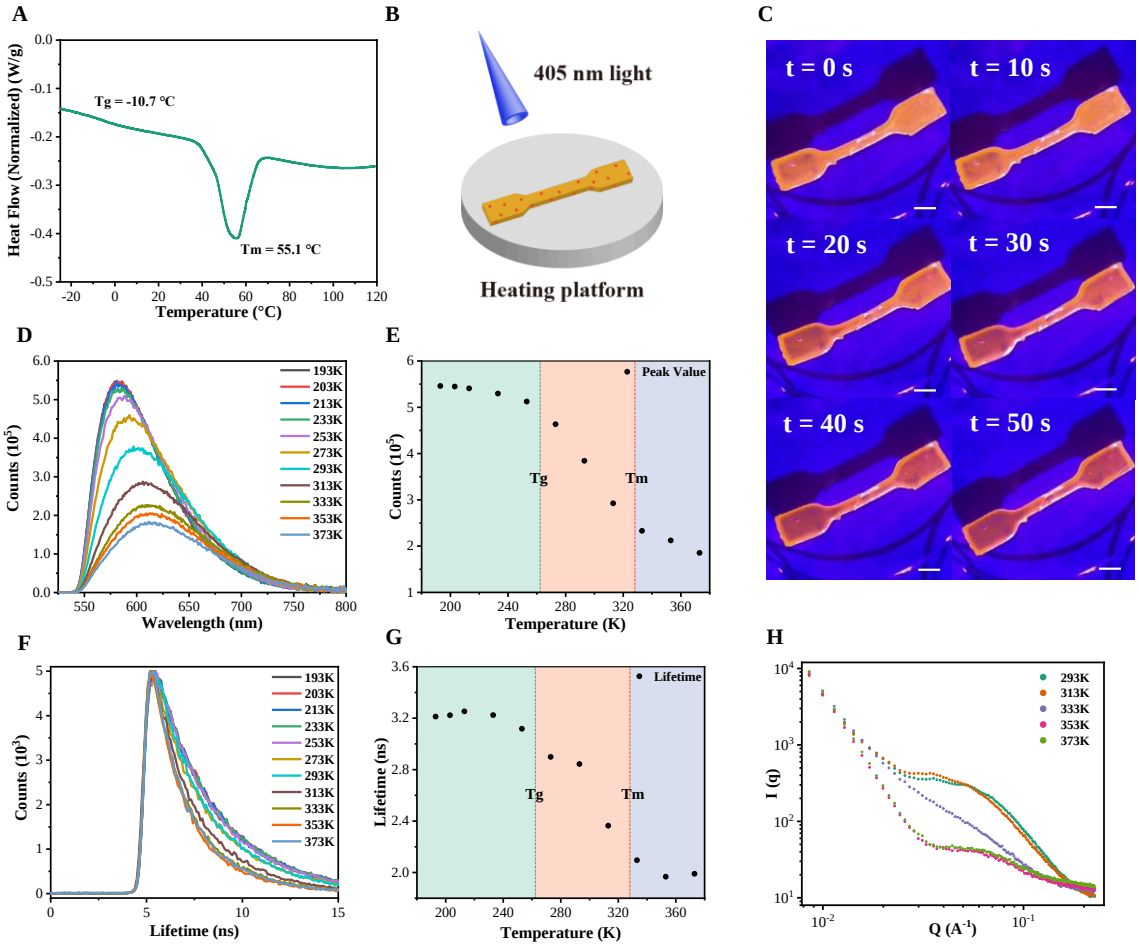

Figure 3. Temperature-modulated emission of fluorescent elastomers. A) DSC analysis of the fluorescent elastomer. B) Schematic diagram of the sample heated in bright field. C) Images of heated sample under 405 nm light from 0 s to 50 s. Scale bar = 2 mm. D) Temperature-dependent fluorescence spectra of fluorescent elastomers. E) Temperature-dependent maximum emission intensity of fluorescent elastomers. F) Temperature-dependent fluorescence lifetime of fluorescent elastomers. Excitation wavelength = 470 nm; emission band-path = 490-800 nm. G) Temperature-dependent fluorescence lifetime spectra of fluorescent elastomers. H) SAXS patterns at temperature from 293 K to 373 K.

In comparison, in between T_g and T_m, the polymer network undergoes a notable internal transformation from rigid to pliable domains. The increased polymer chain mobility provides ample free volume leading to enhanced molecular motions. As a result, the emission intensity reduction was proportional to the temperature. Similar observation was also reported in previous studies that a consistent decrease in film fluorescence intensity with increasing temperature, with a significant change observed at the T_g[53]. Finally, above T_m, the intensity featured a gradual decay due to the further enhanced chain mobility and intramolecular motion. Lower fluorescence intensity of AIE molecules in polymers have

been observed previously under high temperature conditions. An increase in temperature induces more active molecule mobility, while it also leads to a lower polymer viscosity, causing polymer chains to exhibit a less constrained conformation[66,67]. With sufficient volume, molecular mobility increased, contributing to the decrease in AIEgen emission intensity. Additionally, a red shift from 575 nm to 615 nm in the fluorescence profile was observed as the temperature increased from 193 K to 373 K. The rising temperature may intensify the rotation and vibration of the TPAPY-SH enhancing the twisted intramolecular charge transfer and thus triggered the peak shifts[68].

Probing the nanoscale crystalline structures

To quantitatively investigate the correlation between AIEgen emission and the nanoscale structure of our 3D printed materials, *in situ* SAXS experiments were performed at varying temperatures. As depicted in Figure 3H, at a lower temperature of 293 K, an obvious broad scattering peak emerged at 0.035 $Å^{-1}$, corresponding to a domain size of approximately 18 nm, which is in line with the reported lamella packing of PU crystalline domains. This distinct scattering feature indicates the presence of ordered crystalline domains within the 3D printed PU structure when the temperature is below its T_m. As the temperature climbed to 313 K, the primary scattering peak maintained its position, yet the appearance of scattering at higher q angles suggested a reduction in the crystalline domain's ordering. While this change was subtle, the reduction in fluorescence intensity was notably more pronounced. This behavior implies that the AIE probe exhibits remarkable sensitivity to minor variations in crystalline domains, as the polymer network's ordering significantly influences the constrained conformation of AIE molecules.

Approaching the T_m, the SAXS data at 333 K displayed a lack of crystalline domain features, corroborating findings from DSC data. Further increasing the temperature to 353 K and 373 K, SAXS curves revealed analogous patterns with a broad peak around 0.065 $Å^{-1}$, signifying a feature size of 9.7 nm. This observation aligns with the trend evident in Figure 3E indicating that above the T_m, the emission intensity of TPAPY-SH appeared less influenced by temperature changes. These data elucidate that the responsiveness of TPAPY-SH closely tracks the nanoscale structural fluctuations within the 3D printed PU polymer networks. As a result, our AIEgen functions as a highly effective

molecular probe, sensitively capturing alterations in polymer architecture. In summary, these SAXS findings further validate the TPAPY-SH 's capability to act as an efficient probe for the internal structure of 3D printed materials, providing insights into the nanoscale structure, thereby enriching our understanding of these responsive materials.

Enhanced AIEgen emission under mechanical strain

We went on to test whether the AIEgen could also be utilized to probe the effects of mechanical strains on polymer network structure. As shown in Figure 4A, a customized *in situ* fluorescence monitoring device was designed and built allowing simultaneous analysis together with a tensile texture analyzer (ESM3000 motorized force tester, Mark-10). A 405 nm UV light source, which matched the absorption characteristics of the AIE molecule and reduced the potential unwanted stray light captured by our camera, was utilized as the incident light. A laser with a spot size of 2 mm was chosen according to the size of the stand dumbbell-shaped sample. A laser light source is horizontally fixed at a distance of 15 cm from the sample, with the vertical illumination exactly shine on the center of the stretched specimen. Simultaneously, light intensity data perpendicular to the incident direction were recorded using a CCD camera. The light passed a bandpass filter (400 nm – 830 nm) and a high pass filter (480 nm – 1000 nm) before reaching the camera. The images of the 3D printed materials under different strains (0%, 50%, 100%, 150%, and the moment before the fracture) were then acquired and analyzed. As shown in Figure 4B, the fluorescence emission at different positions of the specimen could be directly visualized. An image analysis algorithm was then utilized to integrate the regions of interests (ROI), spanning a region of 3 × 198 pixels located precisely along the central axis, starting from the lower edge of the fixture. The integrated number was thus utilized to quantify the fluorescence intensity under different strains. Briefly, the pixel values of selected ROI were quantified using a MATLAB program. The intensity values ranged from 0 to 255, signifying the absence of light (0) and the brightest region (255). None of the intensity values extracted through MATLAB reached 255, providing evidence of the absence of saturation within ROI. The normalization process involved referencing the value obtained under 0% strain conditions.

As shown in Fig 4B, the 3D printed PU materials exhibited excellent elasticity, characterized by a

Young's modulus of 2.7 ± 0.02 MPa and an elongation of approximately 200%. Meanwhile, a significant increase in the fluorescent intensity could be observed with the increased strain (Figure 4C, 4D) Specifically, without any strain, the integral fluorescent intensity was recorded to be 18119. In sharp contrast, the intensity increased to 19904, 20234, 21214, and 22858 at 50%, 100%, 150%, and 191%, respectively.

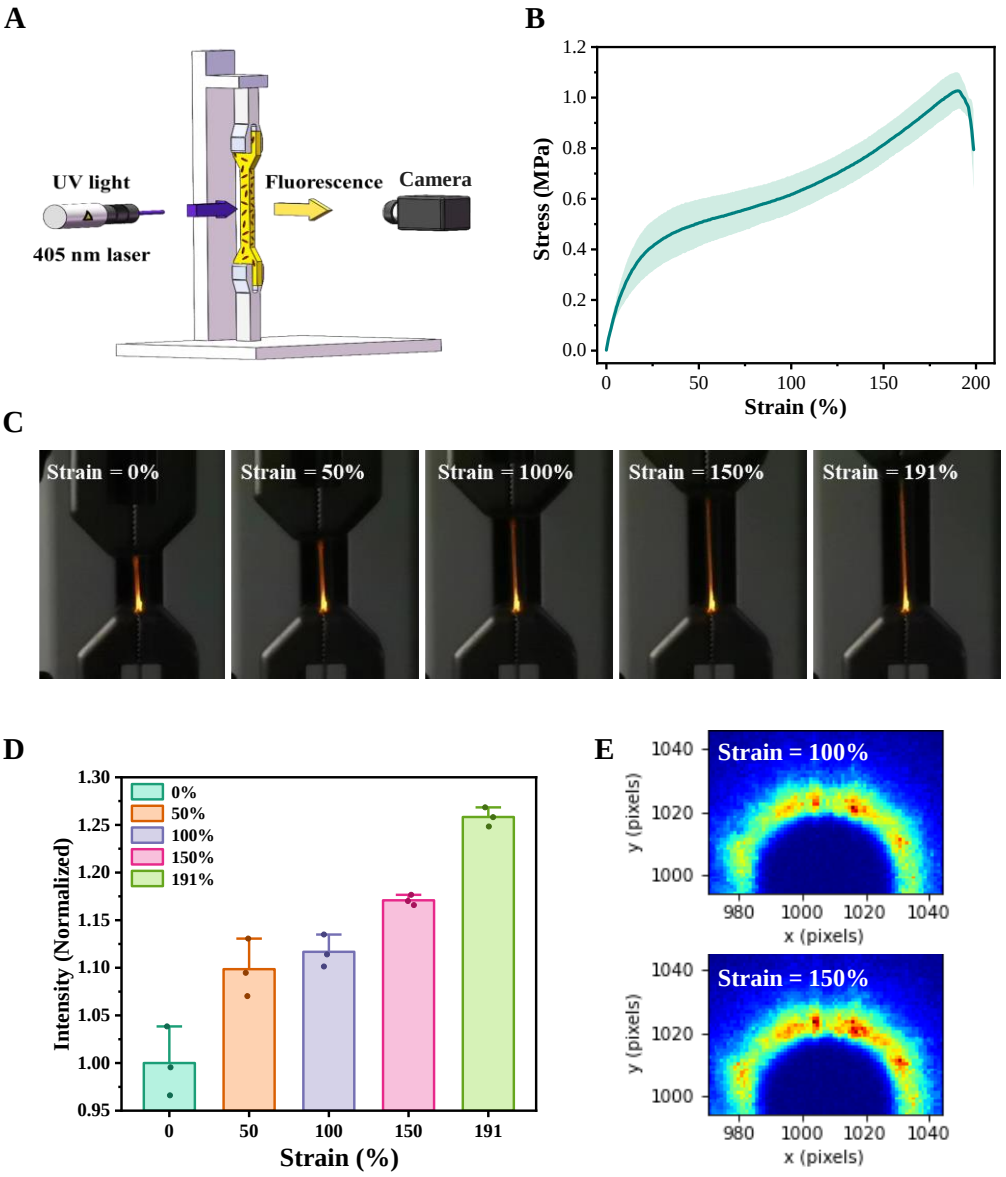

Figure 4. Mechanical strain-dependent emission of fluorescent elastomers. A) Device setup for in situ measurement of the fluorescence intensity during stretching. B) Tensile test of the printed elastomer. C) Images of dumbbell-shape sample at strains of 0%, 50%, 100%, 150% and 191%. D) Normalized fluorescence intensity at different strains. E) 2D SAXS pattern of the elastomer at strain of 100%, and 150%.

Such an obvious enhancement is affected by multiple factors. First of all, mechanical deformation causes polymer chains to align more orderly along the direction of force applied, leading to the restricted intermolecular motion of the AIE molecule[69]. π-π stacking of AIE molecules might be impacted by the shrinkage of the intermolecular space, resulting in the reduced electronic coupling and enhanced emission efficiency[70]. On the other hand, the enhancement of emission intensity may also arise from scattering[71]. A portion of emitted light scattered when travelling through the sample due to the lower refractive index of the film compared to that of air. The scattering diminished the number of photons generated and detected in the central region of the film disrupting the waveguide effect and elevating the detected emission value.

To further understand the mechanism of enhanced AIEgen emission upon mechanical strain, 2D-SAXS analysis was then performed to determine the alignment of the polymer chain. An *in situ* tensile test was performed during the SAXS analysis. The tensile rate was 1 mm/s and the size of the 1-mm thick sample was 30 mm × 8 mm. As shown in Figure 4E, a more heterogeneous scattering patterns were recorded after stretching of the dumbbell-shaped specimen, indicating a higher alignment of polymer chains within the network. This result validates our hypothesis that the decreased free volume in the polymer network induced a more restricted microscopic conformation of the AIE molecules, resulting in enhanced fluorescence intensity. These findings again prove that the AIEgen approach could provide a valuable to visualize the polymer chain organization in 4D materials with external mechanical loading.

Correlation between pH responsiveness and the AIEgen emission

We further investigated the pH-responsiveness of the printed PU material. To illustrate the acid induced swelling effect, square-shaped films measuring 3 mm × 3 mm in dimension were immersed in a hydrochloric acid solution of pH = 1 (Figure 5A). Upon immersion, the samples rapidly expanded to 6 mm × 6 mm within 120 seconds, and the swelling degree exceeded 250% after 4 minutes, indicating substantial polymer chain relaxation and expansion in the acidic environment. Moreover, the 3D printed materials showed decreased swelling when the sample was incubated in a solution with a pH of 3, as well as pH 9 and pH 13 alkaline buffer solution (Figure S7).

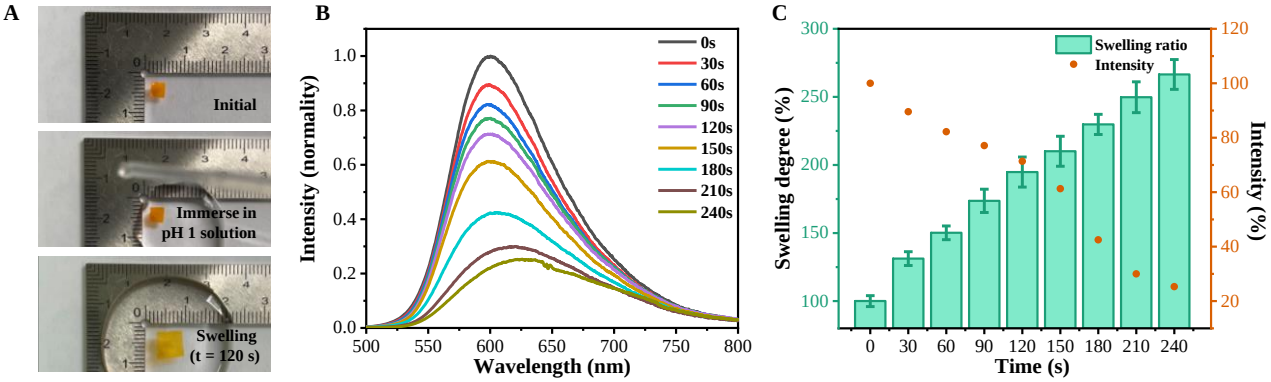

Figure 5. pH-responsive emission of fluorescent elastomers. A. Images of fluorescent elastomer from initial to swelled state. B. Time-dependent fluorescence intensity at solution of pH = 1. C. Time-dependent swelling degree and fluorescence intensity.

The influence of pH on the fluorescence emission intensity was then also investigated in situ. As shown in Figure 5B and 5C, the fluorescent intensity dramatically dropped from 1 to 0.25 (normalized) within 240 seconds. Meanwhile, a linear relationship between expansion degree and fluorescence intensity was observed (Figure S8). Such significant decrease in fluorescence intensity and slight red shift observed under acidic conditions can be attributed to the swelling behavior of the polymer. The acidic environment induces polymer chain relaxation and expansion, resulting in altered intramolecular interactions and changes in the electronic environment surrounding the fluorescent molecules. Theoretically, due to the hydrophobic nature, the aggregation state of TPAPY-SH can also be modulated in water, leading to emission enhancement. However, in this case, the predominant effect on fluorescent intensity appears to stem from the polymer network expansion, which results in reduced spatial constraints on the embedded luminescent units, leading to less restricted molecule rotation. Furthermore, a slight red shift was also observed when the sample swelled. This is due to the reduced restriction of fluorescence molecule motions, leading to more nonradiative decay[72].

Conclusion

In conclusion, this study introduces a novel method that utilizes AIEgen TPAPY-SH as an efficient molecular probe to monitor the dynamics of 3D printed stimuli-responsive materials. By detecting changes in fluorescence intensity or lifetime, AIEgen probes are capable of unveiling intrinsic motions

of 3D printed polymer chains in response to stimuli such as temperature, mechanical, or pH variations. We believe that this approach offers a crucial tool to directly correlate AIEgen emission with molecular-level structural changes and has the potential to reveal the changes in internal structures of 4D printed objects *in operando*. Through systematic experiments involving temperature-modulated emission, mechanical strain, and pH-responsiveness, we establish a clear link between AIE fluorescence and nanoscale structural variations within polymer networks. This novel technique provides insights into the underlying mechanisms of responsiveness in 3D printed materials that were previously unattainable. By enabling direct measurement of material structure changes, our method surpasses traditional techniques of fluorescence imaging and facilitates better design and optimization of 3D printed smart materials for applications spanning from smart or wearable devices to biosensors and beyond.

Materials and Methods

Materials

N-methyldiethanolamine (MDEA, 98%), ethanol, ethyl acetate, hexane, and dichloromethane were purchased from Energy Chemical. Hexamethylene diisocyanate (HDI), 2-Hydroxyethyl Methacrylate (HEMA), and *N, N*-Dimethylformamide (DMF, extra dry) were purchased from J&K. *N*-vinylpyrrolidone (NVP), 4-methylpyridine, piperidine, vitamin E, and 4-(*N*, *N*-diphenyl amino)benzaldehyde were purchased from TCI. Phenylbis (2,4,6-trimethylbenzoyl)-phosphine oxide (BAPO) was purchased form Maclin. Sudan I was purchased from Acros Organics. All the chemicals used as supplied without further purification. Filters were purchased from Shenzhen Zhonglai Technology Co., Ltd.

AIEgen synthesis

The synthesis of AIEgen TPAPY-SH is shown in the schematic diagram of the support material.

Synthesis of **a**[73]. A mixture of 1, 6-dibromohexane (4.82 g, 20 mmol) and potassium thioacetate (1.14 g, 10 mmol) in anhydrous THF was heated at reflux temperature for 12 h under N_2. After cooling to

room temperature, the solution was filtered. The filtrate was evaporated in vacuo, and the residue was purified by column chromatography using DCM and hexane (1:10, v/v) to give pure product S-(6-bromohexyl)ethanethioate (1.43 g, 60%) as colorless oil[74]. ^{1}H NMR (400 MHz, $CDCl_3$) δ 3.38 (t, J = 6.8 Hz, 2H), 2.84 (t, J = 7.2 Hz, 2H), 2.30 (s, 3H), 1.91 – 1.69 (m, 2H), 1.63 – 1.52 (m, 2H), 1.48 – 1.33 (m, 4H). ^{13}C NMR (100 MHz, $CDCl_3$) δ 195.97, 33.81, 32.65, 30.73, 29.43, 29.02, 27.96, 27.72. Then a solution of S-(6-bromohexyl)ethanethioate (1.19 g, 5.0 mmol) and 4-methylpyridine (465 mg, 5.0 mmol) in acetonitrile (10 mL) was heated to reflux for 24 h. The mixture was then allowed to cool to room temperature and concentrated by the rotary evaporator to give colorless oil **a** without a further purification.

Synthesis of **c**. A solution of 4-(diphenyl amino) benzaldehyde (546 mg, 2.0 mmol) and **a** (662 mg, 2.0 mmol) was refluxed under nitrogen in dry ethanol (30 mL) catalyzed by a few drops of piperidine overnight. After cooling to room temperature, the mixture was poured into diethyl ether. The residue was purified by a neutral aluminum oxide column using DCM and MeOH (99:1, v/v) as eluting solvent to give red powder of **c** (498 mg, 85% of yield). ^{1}H NMR (400 MHz, $CDCl_3$) δ 9.15 (d, J = 6.8 Hz, 2H), 7.96 (d, J = 6.8 Hz, 2H), 7.65 (d, J = 16.0 Hz, 1H), 7.48 (d, J = 8.8 Hz, 2H), 7.35 – 7.27 (m, 5H), 7.16 – 7.11 (m, 6H), 7.00 (d, J = 8.8 Hz, 2H), 4.78 (t, J = 7.6 Hz, 2H), 2.81 (t, J = 7.2 Hz, 2H), 2.30 (s, 3H), 2.01 – 1.95 (m, 2H), 1.57 – 1.50 (m, 2H), 1.40 (t, J = 7.2 Hz, 4H). ^{13}C NMR (100 MHz, $CDCl_3$) δ 196.05, 153.77, 150.66, 146.39, 143.94, 141.94, 129.87, 129.62, 127.07, 125.79, 124.61, 123.38, 120.91, 119.03, 77.38, 77.06, 76.75, 60.36, 31.49, 30.69, 29.18, 28.76, 28.01, 25.48.

Synthesis of TPAPY-SH**.** A solution of **c** (293 mg, 0.5 mmol) was dissolved in 1 mL MeOH and refluxed in 1M HCl (10 mL) under nitrogen overnight. After cooling to room temperature, the mixture was neutralized and extracted by DCM. The residue was purified by a neutral aluminum oxide column using DCM and MeOH (50:1, v/v) as eluting solvent to give red powder of TPAPY-SH (386 mg, 71% of yield). ^{1}H NMR (400 MHz, $CDCl_3$) δ 9.19 (dd, J = 4.8 Hz, 2H), 7.93 (dd, J = 12.0, 4.8 Hz, 2H), 7.62 (d, J = 16.0 Hz, 1H), 7.46 (d, J = 8.4 Hz, 2H), 7.31 (m, 5H), 7.16 – 7.10 (m, 6H), 7.00 (t, J = 8.0 Hz, 2H), 4.80 (dd, J = 16.8, 9.6 Hz, 2H), 2.67 (t, J = 6.8 Hz, 1H), 2.50 (m, 1H), 2.07 – 2.01 (m, 2H), 1.69 – 1.58 (m, 2H), 1.50 – 1.39 (m, 4H), 1.25 (s, 1H). ^{13}C NMR (100 MHz, $CDCl_3$) δ 153.70, 150.70,

146.58, 144.36, 141.82, 129.97, 129.93, 129.77, 129.74, 127.31, 126.45, 125.97, 124.81, 124.68, 123.58, 121.14, 121.03, 119.31, 77.48, 77.36, 77.16, 76.84, 39.30, 33.62, 29.00, 27.75, 25.80, 24.54.

AIEgen Characterization

^{1}H and ^{13}C NMR spectra were recorded on a Bruker AVANCE NEO 400. Mass spectra were obtained by ACQUITY UPLC H-Class PLUS/QDa (WATERS) or Q Exactive (Thermo Fisher). Absorption spectra were measured on a Cary 60 UV-Vis (Agilent Technologies). Fluorescence spectra were performed on F-4700 spectrofluorometer (Hitachi, Tokyo, Japan) and FLS 1000 spectrofluorometer (Edinburgh Instruments Ltd., UK).

Polymer synthesis

MDEA (20 g, 167.84 mol) was dissolved in 40 mL dry DMF in an ice bath, followed by the addition of HDI (27.5 mL, 1.02 eq) under stirring. The mixed solution was stirred for 4 hours with parafilm sealed. Then, HEMA (2 g, 0.1 eq) was added to the solution and the reaction was running overnight in a sealed round-bottom flask protected from light at 40 °C. Afterwards, HEMA (1 g, 0.05 eq) was added to the solution and stirred for another 2 hours. The reaction mixture was precipitated in ethyl acetate and hexane (1:1) mixture for 3 times. Next, 0.1 % vitamin E was added as inhibitor to prevent premature crosslinking. The washing mixture was added again to finally precipitate the polymers. Polymers were washed with pure ethyl acetate and dried using rotary evaporation. After vacuumed overnight, 47.2 g white powder was obtained.

Polymer Characterization

1H-NMR spectra were recorded on Bruker AVANCE NEO 400 spectrometer using $CDCl_3$ as solvents. DSC analysis was performed using DSC 2500 from TA Instruments. The samples (ca. 5 mg) were place on the Tzero Aluminum pan and exposed to cool-heat-cool cycles from -40 °C to 120 °C under nitrogen flow (40 mL min^{-1}) protection with cooling rate of 20 °C min^{-1} and heating rate 5 °C min^{-1}. Data were analyzed using TA Instruments Trios software (V5. 4. 0. 300). Small-angle X-rays scattering (SAXS) were obtained using a Bruker NanoSTAR instrument (Brucker AXS GmbH, Karlsruhe,

Germany) equipped with a VANTEC-2000 detector and pinhole collimation system for point focus geometry. 1D profiles were extracted using Origin and 2D profiles were extracted using BioXTAS RAW v2. 1. 4[75].

DLP 3D printing

The DLP resins were prepared by mixing the polyurethane (7 g), NVP (3 g), BAPO (0.1 wt%), Sudan I (0.003 wt%), and vitamin E (0.3 wt%) in a brown vial and stirring at 70 ℃ until the mixture was well blended. The STL files for 3D printing were designed with SOLIDWORKS and Tinkercad. The printing was performed at temperature of 90 ℃ using a digital light processing (DLP) 3D printing system with a 405 nm LED Anycubic Photon MONO X, with layer thickness of 50 μm and exposure time of 30 s. The printed specimens were sonicated in ethanol for 5 minutes to remove the uncured resin adjacent to samples. After dried in the oven, specimens were post-cured in a UV chamber with a 405-nm light source for 10 minutes.

Sample fabrication

TPAPY-SH (10 mg) was dissolved into ethanol (40 mL). The printed samples were pre-heated at 40 °C in the oven for 30 minutes and immersed into the solution. Next, the whole system was sonicated for 10 minutes and soaked for another 30 minutes. The sample with TPAPY-SH then dried in the oven.

Fluorescence test

The temperature-dependent emission and lifetime of 3D printed polyurethane film with TPAPY-SH was measured using FLS 1000 spectrofluorometer (Edinburgh Instruments Ltd., UK) attached with a OptistatDN cryostat (cooled by liquid helium; Oxford Instruments, UK) from 193 K to 373 K and the temperature was controlled using Fluoracle software. The pH-dependent emission of the film was measured using F-4700 spectrofluorometer (Hitachi, Tokyo, Japan). The emission spectra of the sample were collected every 30 seconds for 4 minutes.

Mechanical characterization

Tensile tests were performed on dog-bone shaped specimens with a gauge length of 12 mm, using ESM303 motorized force tester (Mark-10, USA) by under the pulling speed of 1 mm/min. The polyurethane was tested at least three times at room temperature. Young's modulus (E) was determined according to Eq. 1,

$$E = \frac{\sigma}{\varepsilon} \quad (1)$$

where σ is the stress and ε is the strain.

Post-printing swelling

The sample swelling was conducted in a mixing hydrochloric acid solution with potassium chloride of pH = 1 for 4 minutes at ambient temperature. The swelling degree was calculated following Eq. 2,

$$Swelling\ degree = \frac{w - w_0}{w_0} \times 100\% \quad (2)$$

where w_0 is the original weight of the sample, and w is the swelled weight at different sampling points.

Reference

[1] E. MacDonald, R. Wicker, *Science* **2016**, *353*, aaf2093.

[2] D. K. Patel, A. H. Sakhaei, M. Layani, B. Zhang, Q. Ge, S. Magdassi, *Adv. Mater.* **2017**, *29*, 1606000.

[3] S. Tibbits, *Archit. Des.* **2014**, *84*, 116.

[4] Q. Ge, H. J. Qi, M. L. Dunn, *Appl. Phys. Lett.* **2013**, *103*, 131901.

[5] R. L. Truby, J. A. Lewis, *Nature* **2016**, *540*, 371.

[6] X. Kuang, D. J. Roach, J. Wu, C. M. Hamel, Z. Ding, T. Wang, M. L. Dunn, H. J. Qi, *Adv. Funct. Mater.* **2019**, *29*, 1805290.

[7] M. C. Biswas, S. Chakraborty, A. Bhattacharjee, Z. Mohammed, *Adv. Funct. Mater.* **2021**, *31*, 2100257.

[8] N. Paunović, J. Marbach, Y. Bao, V. Berger, K. Klein, S. Schleich, F. B. Coulter, N. Kleger, A. R. Studart, D. Franzen, Z. Luo, J. Leroux, *Adv. Sci.* **2022**, *9*, 2200907.

[9] Y. Bao, N. Paunović, J. Leroux, *Adv. Funct. Mater.* **2022**, *32*, 2109864.

[10] Y. Wang, X. Li, *Compos. Pt. B-Eng.* **2021**, *211*, 108644.

[11] M. Milazzo, F. Libonati, *Adv. Intell. Syst.* **2022**, *4*, 2100278.

[12] D. Chen, Q. Liu, Z. Han, J. Zhang, H. Song, K. Wang, Z. Song, S. Wen, Y. Zhou, C. Yan, Y. Shi, *Adv. Sci.* **2020**, *7*, 2000584.

[13] T. J. Wallin, J. Pikul, R. F. Shepherd, *Nat. Rev. Mater.* **2018**, *3*, 84.

[14] J. D. Hubbard, R. Acevedo, K. M. Edwards, A. T. Alsharhan, Z. Wen, J. Landry, K. Wang, S. Schaffer, R. D. Sochol, *Sci. Adv.* **2021**, *7*, eabe5257.

[15] M. Bodaghi, A. R. Damanpack, W. H. Liao, *Mater. Des.* **2017**, *135*, 26.

[16] X. Xin, L. Liu, Y. Liu, J. Leng, *Adv. Funct. Mater.* **2020**, *30*, 2004226.

[17] X. Xia, C. M. Spadaccini, J. R. Greer, *Nat. Rev. Mater.* **2022**, *7*, 683.

[18] C. L. C. Chan, J. M. Taylor, E. C. Davidson, *Nat. Synth.* **2022**, *1*, 592.

[19] Z. Dong, H. Cui, H. Zhang, F. Wang, X. Zhan, F. Mayer, B. Nestler, M. Wegener, P. A. Levkin, *Nat. Commun.* **2021**, *12*, 247.

[20] P. Liu, X. Chen, G. Wang, *Matter* **2021**, *4*, 3374.

[21] S. R. Dabbagh, M. R. Sarabi, M. T. Birtek, S. Seyfi, M. Sitti, S. Tasoglu, *Nat. Commun.* **2022**, *13*, 5875.

[22] D. G. Moore, L. Barbera, K. Masania, A. R. Studart, *Nat. Mater.* **2020**, *19*, 212.

[23] Z. Wang, M. Heck, W. Yang, M. Wilhelm, P. A. Levkin, *Adv. Funct. Mater.* **2023**, 2300947.

[24] B. Deore, K. L. Sampson, T. Lacelle, N. Kredentser, J. Lefebvre, L. S. Young, J. Hyland, R. E. Amaya, J. Tanha, P. R. L. Malenfant, H. W. De Haan, C. Paquet, *Nat. Commun.* **2021**, *12*, 55.

[25] M. K. McBride, A. M. Martinez, L. Cox, M. Alim, K. Childress, M. Beiswinger, M. Podgorski, B. T. Worrell, J. Killgore, C. N. Bowman, *Sci. Adv.* **2018**, *4*, eaat4634.

[26] C. De Pascali, G. A. Naselli, S. Palagi, R. B. N. Scharff, B. Mazzolai, *Sci. Robot.* **2022**, *7*, eabn4155.

[27] L. Zu, J. Wen, S. Wang, M. Zhang, W. Sun, B. Chen, Z. L. Wang, *Sci. Adv.* **2023**, *9*, eadg5152.

[28] H. Liu, H. Zhang, W. Han, H. Lin, R. Li, J. Zhu, W. Huang, *Adv. Mater.* **2021**, *33*, 2004782.

[29] A. M. Bellinger, M. Jafari, T. M. Grant, S. Zhang, H. C. Slater, E. A. Wenger, S. Mo, Y.-A. L. Lee, H. Mazdiyasni, L. Kogan, R. Barman, C. Cleveland, L. Booth, T. Bensel, D. Minahan, H. M.

Hurowitz, T. Tai, J. Daily, B. Nikolic, L. Wood, P. A. Eckhoff, R. Langer, G. Traverso, *Sci. Transl. Med.* **2016**, *8*.
[30] R. Raman, T. Hua, D. Gwynne, J. Collins, S. Tamang, J. Zhou, T. Esfandiary, V. Soares, S. Pajovic, A. Hayward, R. Langer, G. Traverso, *Sci. Adv.* **2020**, *6*, eaay0065.
[31] A. Lendlein, R. Langer, *Science* **2002**, *296*, 1673.
[32] S. Babaee, S. Pajovic, A. R. Kirtane, J. Shi, E. Caffarel-Salvador, K. Hess, J. E. Collins, S. Tamang, A. V. Wahane, A. M. Hayward, H. Mazdiyasni, R. Langer, G. Traverso, *Sci. Transl. Med.* **2019**, *11*, eaau8581.
[33] A. Ghosh, L. Li, L. Xu, R. P. Dash, N. Gupta, J. Lam, Q. Jin, V. Akshintala, G. Pahapale, W. Liu, A. Sarkar, R. Rais, D. H. Gracias, F. M. Selaru, *Sci. Adv.* **2020**, *6*, eabb4133.
[34] J. Li, J. A. Viveros, M. H. Wrue, M. Anthamatten, *Adv. Mater.* **2007**, *19*, 2851.
[35] J. N. Chu, G. Traverso, *Nat. Rev. Gastroenterol. Hepatol.* **2022**, *19*, 219.
[36] N. Paunović, D. Meyer, A. Krivitsky, A. R. Studart, Y. Bao, J.-C. Leroux, *J. Control. Release* **2023**, *361*, 417.
[37] X. Xu, J. Wu, Y. Liu, M. Yu, L. Zhao, X. Zhu, S. Bhasin, Q. Li, E. Ha, J. Shi, O. C. Farokhzad, *Angew. Chem. Int. Ed. Engl* **2016**, *55*, 7091.
[38] Y. Shmueli, Y.-C. Lin, S. Lee, M. Zhernenkov, R. Tannenbaum, G. Marom, M. H. Rafailovich, *ACS Appl. Mater. Interfaces* **2019**, *11*, 37112.
[39] A. Nogales, E. Gutiérrez-Fernández, M.-C. García-Gutiérrez, T. A. Ezquerra, E. Rebollar, I. Šics, M. Malfois, S. Gaidukovs, E. Gēcis, K. Celms, G. Bakradze, *Macromolecules* **2019**, *52*, 9715.
[40] A. Rodriguez-Palomo, V. Lutz-Bueno, M. Guizar-Sicairos, R. Kádár, M. Andersson, M. Liebi, *Addit. Manuf.* **2021**, *47*, 102289.
[41] C. Ma, T. Li, Q. Zhao, X. Yang, J. Wu, Y. Luo, T. Xie, *Adv. Mater.* **2014**, *26*, 5665.
[42] R. T. K. Kwok, C. W. T. Leung, J. W. Y. Lam, B. Z. Tang, *Chem. Soc. Rev.* **2015**, *44*, 4228.
[43] J. Qian, B. Z. Tang, *Chem* **2017**, *3*, 56.
[44] Z. Wang, Y. Zhou, R. Xu, Y. Xu, D. Dang, Q. Shen, L. Meng, B. Z. Tang, *Coord. Chem. Rev.* **2022**, *451*, 214279.
[45] T. Bu, T. Xiao, Z. Yang, G. Liu, X. Fu, J. Nie, T. Guo, Y. Pang, J. Zhao, F. Xi, C. Zhang, Z. L. Wang, *Adv. Mater.* **2018**, *30*, 1800066.
[46] H. Wang, E. Zhao, J. W. Y. Lam, B. Z. Tang, *Mater. Today* **2015**, *18*, 365.
[47] F. Würthner, *Angew. Chem. Int. Ed.* **2020**, *59*, 14192.
[48] Y. Tu, Z. Zhao, J. W. Y. Lam, B. Z. Tang, *Natl. Sci. Rev.* **2021**, *8*, nwaa260.
[49] J. Zhang, B. He, W. Wu, P. Alam, H. Zhang, J. Gong, F. Song, Z. Wang, H. H. Y. Sung, I. D. Williams, Z. Wang, J. W. Y. Lam, B. Z. Tang, *J. Am. Chem. Soc.* **2020**, *142*, 14608.
[50] S. Zhang, J. Yan, A. Qin, J. Sun, B. Z. Tang, *Sci. China Chem.* **2013**, *56*, 1253.
[51] S. Ye, T. Tian, A. J. Christofferson, S. Erikson, J. Jagielski, Z. Luo, S. Kumar, C.-J. Shih, J.-C. Leroux, Y. Bao, *Sci. Adv.* **2021**, *7*, eabd1794.
[52] S. Ye, N. Meftahi, I. Lyskov, T. Tian, R. Whitfield, S. Kumar, A. J. Christofferson, D. A. Winkler, C.-J. Shih, S. Russo, J.-C. Leroux, Y. Bao, *Chem* **2023**, *9*, 924.
[53] Z. Qiu, E. K. K. Chu, M. Jiang, C. Gui, N. Xie, W. Qin, P. Alam, R. T. K. Kwok, J. W. Y. Lam, B. Z. Tang, *Macromolecules* **2017**, *50*, 7620.

[54] H. Liu, B. Liu, L.-C. Lin, G. Chen, Y. Wu, J. Wang, X. Gao, Y. Lv, Y. Pan, X. Zhang, X. Zhang, L. Yang, C. Sun, B. Smit, W. Wang, *Nat. Commun.* **2014**, *5*, 5147.
[55] Q. Lai, S. Toan, M. A. Assiri, H. Cheng, A. G. Russell, H. Adidharma, M. Radosz, M. Fan, *Nat. Commun.* **2018**, *9*, 2672.
[56] N. Paunović, Y. Bao, F. B. Coulter, K. Masania, A. K. Geks, K. Klein, A. Rafsanjani, J. Cadalbert, P. W. Kronen, N. Kleger, A. Karol, Z. Luo, F. Rüber, D. Brambilla, B. von Rechenberg, D. Franzen, A. R. Studart, J.-C. Leroux, *Sci. Adv.* **2021**, *7*, eabe9499.
[57] M. Zarek, M. Layani, I. Cooperstein, E. Sachyani, D. Cohn, S. Magdassi, *Adv. Mater.* **2016**, *28*, 4449.
[58] M. Zarek, M. Layani, S. Eliazar, N. Mansour, I. Cooperstein, E. Shukrun, A. Szlar, D. Cohn, S. Magdassi, *Virtual Phys. Prototyp.* **2016**, *11*, 263.
[59] M. Zarek, N. Mansour, S. Shapira, D. Cohn, *Macromol. Rapid Commun.* **2017**, *38*, 1600628.
[60] B. Steyrer, B. Busetti, G. Harakály, R. Liska, J. Stampfl, *Addit. Manuf.* **2018**, *21*, 209.
[61] M. Kang, C. Zhou, S. Wu, B. Yu, Z. Zhang, N. Song, M. M. S. Lee, W. Xu, F.-J. Xu, D. Wang, L. Wang, B. Z. Tang, *J. Am. Chem. Soc.* **2019**, *141*, 16781.
[62] Y. Bao, E. Guégain, V. Nicolas, J. Nicolas, *Chem. Commun.* **2017**, *53*, 4489.
[63] M. H. Cohen, D. Turnbull, *J. Chem. Phys.* **1959**, *31*, 1164.
[64] G. Adam, J. H. Gibbs, *J. Chem. Phys.* **1965**, *43*, 139.
[65] C. B. Roth, J. R. Dutcher, *J. Electroanal. Chem.* **2005**, *584*, 13.
[66] H. S. Kumbhar, S. S. Deshpande, G. S. Shankarling, *ChemistrySelect* **2016**, *1*, 2058.
[67] Y. Zhang, S. Wang, X. Wang, Q. Zan, X. Yu, L. Fan, C. Dong, *Anal. Bioanal. Chem.* **2021**, *413*, 3823.
[68] X. Yang, R. Lu, H. Zhou, P. Xue, F. Wang, P. Chen, Y. Zhao, *Journal of Colloid and Interface Science* **2009**, *339*, 527.
[69] V. A. Dini, A. Gradone, M. Villa, M. Gingras, M. L. Focarete, P. Ceroni, C. Gualandi, G. Bergamini, *Chem. Commun.* **2023**, *59*, 1465.
[70] L. Zong, Y. Xie, C. Wang, J.-R. Li, Q. Li, Z. Li, *Chem. Commun.* **2016**, *52*, 11496.
[71] V. A. Dini, A. Pucci, D. Genovese, C. Gualandi, C. Micheletti, N. Zaccheroni, *Aggregate* **2023**, *e373*.
[72] W. Guo, S. Ma, H. Wang, L. Qiao, L. Chen, C. Hong, B. Liu, X. Zheng, H. Peng, *Aggregate* **2023**, e415.
[73] H. M. Osorio, S. Catarelli, P. Cea, J. B. G. Gluyas, F. Hartl, S. J. Higgins, E. Leary, P. J. Low, S. Martín, R. J. Nichols, J. Tory, J. Ulstrup, A. Vezzoli, D. C. Milan, Q. Zeng, *J. Am. Chem. Soc.* **2015**, *137*, 14319.
[74] L. Shi, C. Jing, W. Ma, D.-W. Li, J. E. Halls, F. Marken, Y.-T. Long, *Angew. Chem. Int. Ed.* **2013**, *52*, 6011.
[75] J. B. Hopkins, R. E. Gillilan, S. Skou, *J. Appl. Crystallogr.* **2017**, *50*, 1545.

Acknowledgements

X.K. and W.W. contributed equally to this work. This work was supported by the National Key Research and Development Program of China (No. 2022YFB3804700). W.W. acknowledges the Basic and Applied Basic Research Foundation of Guangdong Province (2023A1515011900). Z.L. was supported by Large Scientific Facility Open Subject of Songshan Lake, Dongguan, Guangdong (KFKT2022A09). The authors acknowledge Guangdong Provincial Key Laboratory of Advanced Biomaterials (2022B1212010003). The authors also acknowledge the SUSTech Core Research Facilities for technical support. The authors would like to thank Dr. Huilin Xie from The Hong Kong University of Science and Technology with photoluminescence quantum yield measurement.

Keywords: 3D printing • AIEgen • stimuli-responsive • polymer networks